Demonstration of Auxiliary Management and Control Channel Transmission and Data-Channel Signal Compensation for Beyond 100G FDM Coherent PON

Wangwei Shen[1,2], Jiaye Wang[1,2], Sizhe Xing[1,2], Guoqiang Li[1,2], Zhongya Li[1,2], An Yan[1,2], Ziwei Li[1,2], Chao Shen[1,2], Jianyang Shi[1,2], Nan Chi[1,2] and Junwen Zhang[1,2*]

[1]*Key Laboratory of EMW Information (MoE), Fudan University, Shanghai 200433, China*

[2]*Shanghai ERC of LEO Satellite Communication and Applications, Shanghai CIC of LEO Satellite Communication Technology, Fudan University, Shanghai 200433, China*

E-mail address: junwenzhang@fudan.edu.cn

Abstract: We propose and demonstrate the transmission of AMCC and a novel signal-compensation method for data-channel in coherent FDM-PON. Sensitivity improvement of 6 dB is demonstrated with 150G capacity over 20-km fiber for FDM-PON with AMCC.

1. Introduction

In recent years, emerging network services, including autonomous driving, telemedicine, and intelligent factories, have presented elevated demands in terms of network capacity and latency [1-3]. In the optical access network, frequency division multiplexing passive optical network (FDM-PON) based on coherent optics is one of the candidates to realize such large-capacity and low-latency networks because a frequency channel is exclusively allocated to each user and service [4]. To enable the transmission of control information with minimal latency and preserve the frame structure without any alterations, an embedded communication protocol is necessary. Just like the control information transmission in WDM-PON, we believe that Auxiliary Management and Control Channel (AMCC) can also be an effective method for low latency operations in coherent FDM PON [5].

The AMCC serves as a low-latency control channel that is implemented by superimposing a low-speed control signal on the data-channel signal, utilizing a relatively small modulation index (MI) to effectively mitigate interference on the signal. Numerous demonstrations have reported successful integration of AMCC within IM-DD WDM-PON systems [6-7]. One approach involves controlling the bias voltage of the Mach-Zehnder modulator (MZM) using a non-return-to-zero (NRZ) signal, which is superimposed on the main signal [6]. More recently, there have been demonstrations of superimposing the NRZ signal on the data-channel signal during the digital signal processing (DSP) stage of the transmitter (Tx) in coherent FDM-PON systems [8]. However, prior studies utilizing multiplication-based AMCC have indicated that, when the MI is large, it has a significant impact on the sensitivity of the data-channel signal, resulting in increased penalties [9]. Consequently, exploring methods to mitigate the adverse effects of a large MI on data-channel signal sensitivity represents a critical area of research.

In this paper, we demonstrate the transmission of AMCC and introduce a novel compensation method for the data-channel signal in a coherent FDM-PON. Each subcarrier transmits distinct signals along with AMCC signals, effectively handling both AMCC decoding and signal compensation. As a proof-of-concept, we showcase an AMCC embedded FDM-PON with four subcarriers, achieving up to 6-dB sensitivity improvement and a data rate of 150 Gb/s over a 20-km fiber, even within a 31-dB power-budget.

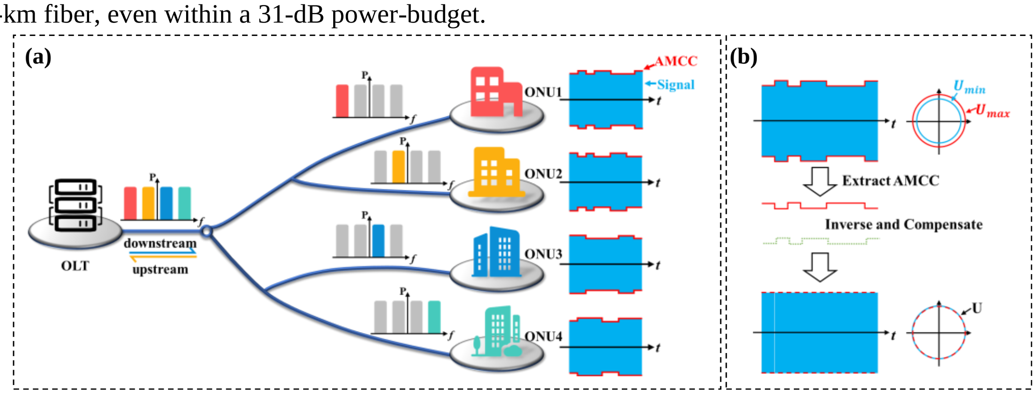

Fig.1 (a) Architecture diagram of FDM-PON. (b) Schematic diagram of compensation algorithm.

2. Principles and Experimental Setup

The architecture diagram of FDM-PON shown in Fig. 1(a). The optical line terminal (OLT) allocates subcarriers to different optical network units (ONUs) in the same time slot, and each subcarrier serves one ONU. Each subcarrier transmits different data-channel signals and NRZ signals. After the AMCC is superimposed with the data-channel signal, the amplitude of the signal will fluctuate, as shown in Fig. 1(b). Upon receiving the signal, AMCC is extracted using envelope detection. Subsequently, an inverse mapping is applied, exchanging t the values that NRZ 0 and 1 were originally mapped to. Inverse-mapping AMCC is then multiplied with the data-channel signal. This process adjusts the signal's amplitude to its original state before being superimposed with the AMCC, effectively compensating for the impact of the AMCC on the data-channel signal.

Fig. 2(a) shows the DSP of Tx. The signal is mapped to 8QAM in each subcarrier and up-sampled 16 times to maintain a consistent sampling rate using a 100-Gsa/s arbitrary waveform generator (AWG). Following that, signal is subjected to shaping filtering using a root raised cosine (RRC) filter with a roll-off factor of 0.1 to enhance the signal-to-noise ratio (SNR). Subsequently, the narrow-bandwidth NRZ signal is up-sampled to align with the number of symbols in the data-channel signal and multiplied with it. Up-convert the signal to different frequency bands and add them to obtain four 6.25-GBaud 8QAM signal as shown in Fig. 2(g) and sent to the AWG for transmission. Fig.2(b) and (c) shows the setups of Tx and Rx, respectively. The four subcarrier signals undergo amplification by a boosted erbium-doped fiber amplifier (EDFA) and are then transmitted through the fiber after passing through a dual polarization (DP) IQ modulator. The DP IQ modulator in this study utilizes an external cavity laser (ECL) with a wavelength of 1553.6 nm and a linewidth of less than 100 kHz. The launch power of the signal is fixed at 0 dBm after passing through the EDFA. Following a 20-km fiber transmission, the signal passes through an attenuator and is received by an integrated coherent receiver (ICR). The ICR's local oscillator (LO) operates at a wavelength of 1553.6 nm with a linewidth of less than 100 kHz. The detected signals are captured by a four channel 40-Gsa/s digital storage oscilloscope (DSO) for offline DSP. Fig. 2(d) shows the DSP of Rx. After achieving frame synchronization, a frame signal is extracted. It is then multiplied with the mirror-mapped NRZ signal to restore the signal's amplitude to its original state before being combined with the AMCC. Fig. 2(e) and (f) shows the time domain waveform of data-channel signal without and with compensation algorithm, respectively. Prior to applying the compensation algorithm, the amplitude of the signal's time-domain waveform exhibits fluctuations. However, after employing the compensation algorithm, the amplitude of the time-domain waveform becomes stable and flat. And then, the signal undergoes the subsequent decoding process.

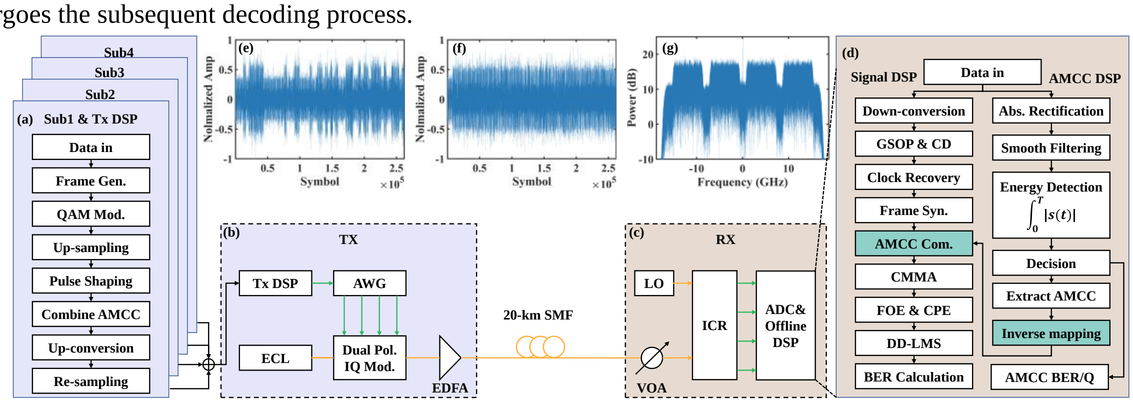

Fig.2 (a) DSP of Tx. (b) and (c) the setups of Tx and Rx, respectively. (d) DSP of Rx. (e) and (f) Time domain waveform of data channel signal without and with compensation algorithm, respectively. (g) The spectrum of four 6.25GBaud 8QAM at Rx

3. Results

To demonstrate the efficacy of the proposed compensation algorithm we tested the sensitivity curve of the data-channel signal at different MI with and without the algorithm. The experimental results of back-to-back (BtB) and 20-km transmission of data-channel are shown in Fig. 3(a) and (b), respectively. In the BtB transmission scenario, sensitivity can be improved by 1.5 dB at MI of 26.1% and 3.5 dB at MI of 40% when using the compensation algorithm. At the same time, in 20-km transmission scenario, the sensitivity of data-channel signal can be improved by 1.2 dB at MI of 26.1% and 3.4dB at MI of 40% when using the compensation algorithm. It can also be seen that when the compensation algorithm is not used, the constellation diagram of the data-channel signal exhibit distortion as shown in (i) and (iii) of Fig. 3(b). When the compensation algorithm is used, the constellation diagram returns to normal as shown in (ii) and (iv) of Fig. 3(b). The Q of AMCC is affected by ROP, as shown in Fig. 3(c). As the ROP increases, the Q value of AMCC will gradually increase.

In addition to ROP, the MI and bandwidth of AMCC also affect the performance of data-channel signal. As shown in Fig. 3(d) and (e), as the MI of AMCC increases, both the sensitivity penalty of the data-channel signal and the Q of AMCC gradually increases. When testing the impact of MI, the ROP was fixed at -28dBm, and the bandwidth of AMCC was fixed at 24.4 MHz. After using the compensation algorithm, the sensitivity of the data-channel signal is improved at any MI. The compensation algorithm can improve the sensitivity of data-channel signal by 6 dB at MI of 46.15%. Meanwhile, the impact of bandwidth on sensitivity of data-channel signal and Q of AMCC is shown in Fig. 3(e). When testing the impact of bandwidth, the ROP was fixed at -28dBm, and the MI of AMCC was fixed at 40%. As the bandwidth of AMCC increases, the sensitivity penalty of the signal increases, and the Q of AMCC decreases. After using the compensation algorithm, the compensation algorithm can improve the sensitivity of data-channel signal by 3.7 dB at bandwidth of 48.8 MHz. These results demonstrate that under the large MI and bandwidth of AMCC, the compensation algorithm can effectively compensate for the impact of AMCC on the data-channel signal.

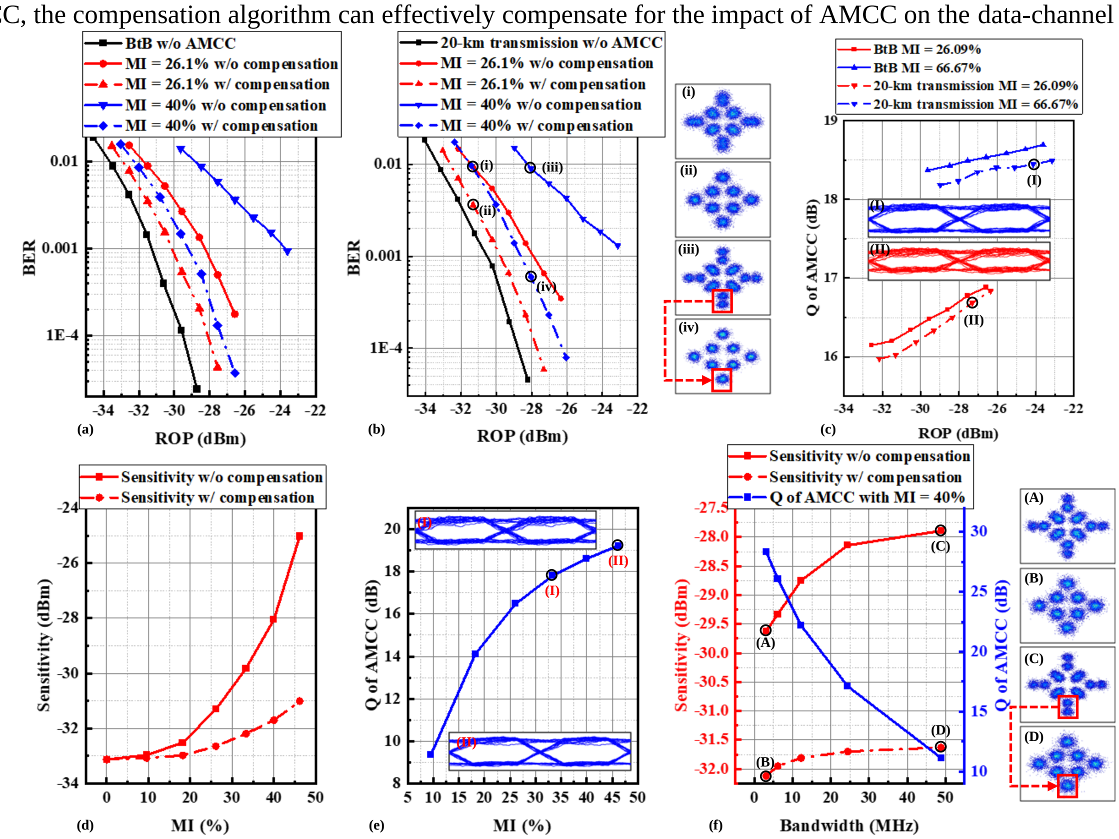

Fig.3 Sensitivity curves of 8QAM data-channel at different MI with and without compensation algorithm in (a) BtB and (b) 20-km transmission. (c) Q of AMCC at different MI in BtB and 20-km transmission. (d) Sensitivity of data-channel versus MI with and without compensation algorithm. (e) Q of AMCC versus MI. (f) Sensitivity of data-channel versus bandwidth with and without compensation algorithm and Q of AMCC versus bandwidth.

4. Conclusions

The transmission of AMCC and a novel compensation algorithm for data-channel signal are experimentally demonstrated. As a proof-of-concept, an AMCC-embedded FDM-PON is demonstrated based on four digital subcarriers, achieving a data rate of 150 Gb/s/λ over 20-km fiber at 31-dB power-budget and sensitivity improvement of up to 6dB based on the proposed compensation algorithm.

Acknowledgement: This work is partially supported by National Natural Science Foundation of China (62171137, 61925104, 62031011), Natural Science Foundation of Shanghai (21ZR1408700).

References

[1] A Delmade, et al., arXiv, 2308.10637(2023)
[2] Q Zhuge, et al., J. Opt. Comm. Netw. 15.8, C242-C262(2023)
[3] R. Igarashi, et al., Optics Express, 30.26, 48030-48041(2022).
[4] J. Zhang, et al., Opt. Fiber Technol, 75, 103190(2023).
[5] ITU-T. Rec. G.989.1 General requirements Amendment 1(2013)
[6] H. Guo, et al., Optics Express, 30.18, 31602-31613(2022).
[7] Y. Tanaka, et al., J. Light Technol., 40.17, 5783-5792(2022).
[8] J. Wang, et al., in OECC 2023, paper 1-3.
[9] W. Shen, et al., in ACP 2023.